Development of a Simple Method to Construct Finite Element Models of Aortas from MRI Images and Its Application to Thoracic Aortic Aneurysm*

Yoko KATO**, Takeo MATSUMOTO**,
Kiichirou KUMAGAI***, Hiroji AKIMOTO***,
Koichi TABAYASHI*** and Masaaki SATO**

We have developed a method to construct finite element models of the whole thoracic aortas from T1-weighted MRI images. Intraluminal shape of the aorta perpendicular to its axis was assumed to be circular. We constructed a normal aortic model from a healthy male. Aneurysm models were made by adding a fusiform bulge to the ascending, arch, or descending regions of the normal model. In the analysis, aortic walls were assumed to be linearly elastic and the inner surface were pressurized at the pulse pressure of the subject. In all models, high stress appeared in the inner and lateral regions of the arch where aneurysm is prone to form. Peak stress in the wall was highest in the model with aneurysm at aortic arch. Eccentricity increased the peak stress. Aneurysms at the arch or with eccentricity have higher risk of rupture. Stress analysis may provide important information on aneurysm treatment.

Key Words: Finite Element Method, Medical Engineering, Biological Engineering, MRI, Aortic Aneurysm, Thoracic

1. Introduction

Aortic aneurysms are generally replaced with aortic prostheses when their maximum diameter exceeds 5 cm. Such criteria are based on clinical experiences and are not always reliable. Aneurysms whose maximum diameter is less than 5 cm rupture in some cases. For the better treatment of aortic aneurysm disease, it is necessary to evaluate the rupture potential of the aneurysm quantitatively.

There have been several studies on the effect of the aneurysm shapes on the stress and stress distribution of aneurysms with finite element analysis[1]-[4]. In most of the studies, however, the actual shape of the aneurysm was not used, but simplified models consisted of a straight tube and a bulge were used frequently. It might be enough for the analysis of the abdominal aortic aneurysm, because the abdominal aorta has relatively simple geometry and can be considered to be a straight tube. But these models can not apply to the aneurysm at the thoracic aorta because the thoracic aorta is not a straight tube and has much more complex geometry than the abdominal aorta. Thus we need to construct realistic models of the thoracic aortas from MRI images.

In this study, we developed a simple method to construct finite element models of the thoracic aorta from T1-weighted MRI images. We applied this method to a healthy male and constructed a model of the normal thoracic aorta. We also made aneurysm models by adding a bulge to the model. Finite element analyses were performed to obtain stress distribution in each model pressurized at the pulse pressure of the subject, and the effects of the aneurysm position and eccentricity on the stress distribution and the maximum value of the stress were evaluated.

2. Method

2.1 Images

We used 34 T1-weighted MRI images obtained

* Received 26th June, 2000

** Biomechanics Laboratory, Graduate School of Engineering, Tohoku University, Aoba-yama 01, Sendai 980-8579, Japan. E-mail : yoko@biomech.mech.tohoku.ac.jp

*** Department of Thoracic and Cardiovascular Surgery, Tohoku University, Seiryou-machi 2-1, Aoba-ku, Sendai 980-8575, Japan

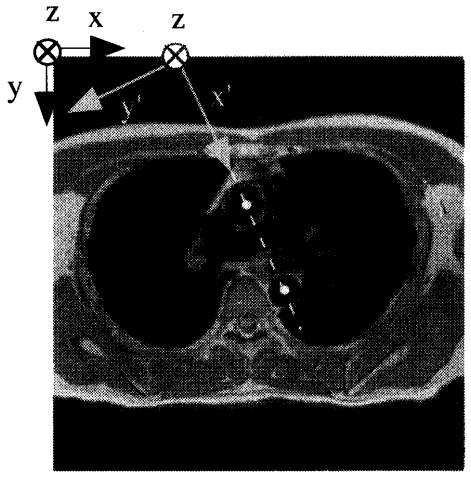

Fig. 1 An example image viewed from the feet. x, y, and z indicate the original coordinate system. x', y', and z indicate the rotated coordinate system. The white points inside of the aortic lumen indicate the centers of gravity of aortic cross sections.

from a 29-year-old healthy male with MAGNETOM Vision 1.5 T (Siemens) in Department of Thoracic and Cardiovascular Surgery, Tohoku University. These images were perpendicular to the body axis, and covered the ascending aorta, the aortic arch, and the descending aorta at intervals of 4 mm. An example image is shown in Fig. 1 along with coordinates set for the analysis.

2. 2 Construction of the normal model

We first tried to identify the shape of the aorta in the MRI images automatically, and it turned out to be very difficult because the boundary between the wall and the lumen was not clear enough for an automatic analysis. We thus obtained the luminal shape of the aorta from the MRI images manually. To grasp the shape of the aorta, we utilized the center of gravity and the inner radius of the aortic lumen in each MRI image. The locus of the center of gravity was used as the centerline of the aorta. We approximated the locus with the combination of three polynomial functions. The change of the radius along the centerline was approximated with another polynomial function to express tapering of the aorta. Three dimensional model of the aorta was constructed as a curved tapered tube with circular cross section from the centerline and the radius change of the aorta. The outline of the construction method is shown in Fig. 2.

2. 2. 1 Digitization of the images The images taken in DICOM format were transferred from the MRI system to a personal computer (Macintosh Quadra 840AV, Apple Computer Inc.) with an optical disk. The format of the image was converted to TIFF on the personal computer using an image analysis software (NIH Image 1.60/68 k) for the image processing with another software (IP Lab Spectrum ver. 2.3, Scanalytics, Inc.) which cannot handle images in DICOM format. The procedure of the digitization is as follows: First, the operator traced the lumen of the aorta in each image with a mouse. Then, the software calculated the position of the center of gravity (x_g, y_g), the eccentricity e, and the area S enclosed by the traced lumen automatically. The eccentricity was calculated using the longest distance l_l and the shortest distance l_s from the center of gravity to the lumen as follows:

$$e=\frac{\sqrt{l_l^2-l_s^2}}{l_l}. \qquad (1)$$

These parameters were used for the construction of 3 dimensional model of the thoracic aorta. We estimated the centerline from (x_g, y_g) of each image in 2.2.2. and r from e and S of each image in 2.2.3.

2. 2. 2 The centerline of the aorta The centerline of the aorta was approximated with polynomial functions. The centers of gravity were considered to be on the same plane in all sections, because the correlation coefficient between their x and y coordinates was more than 0.9. Thus we rotated the coordinate system xyz along z axis and defined new coordinate system $x'y'z$ in which x'-z plane corresponds to the plane of the centers of gravity as shown in Fig. 1 in order to simplify the calculation. The thoracic aorta was divided into three regions, the ascending aorta, the aortic arch, and the descending aorta. In the ascending aorta, we approximated the x coordinate with a cubic polynomial function of the z coordinate using 10 images of the ascending aorta and the aortic arch. Similarly in the descending aorta, the x coordinate was approximated with a 4-degree polynomial function of the z coordinate using 34 images of the descending aorta and the aortic arch. The z coordinate in the aortic arch was approximated with a cubic polynomial function of x coordinate using 4 images of the aortic arch. The range of the images used for each ceterline approximation was overlapped to connect centerlines smoothly. We used least square method for each approximation. The correlation coefficients between the data and the approximation were more than 0.99 for all approximations. The equations we got are as follows:

$$x=-2.393\times10^{-4}z^3+4.086\times10^{-2}z^2-2.230z+342.4 \quad (z: 52\rightarrow16) \qquad (2)$$

for the ascending aorta;

$$z=2.437\times10^{-4}x^3-0.2135x^2+60.86x-5.587\times10^3 \quad (z: 16\rightarrow3\rightarrow16) \qquad (3)$$

for the aortic arch;

$$x=-3.089\times10^{-7}z^4+1.302\times10^{-4}z^3-2.131\times10^{-2}z^2+1.408z+337.3 \quad (z: 16\rightarrow148) \qquad (4)$$

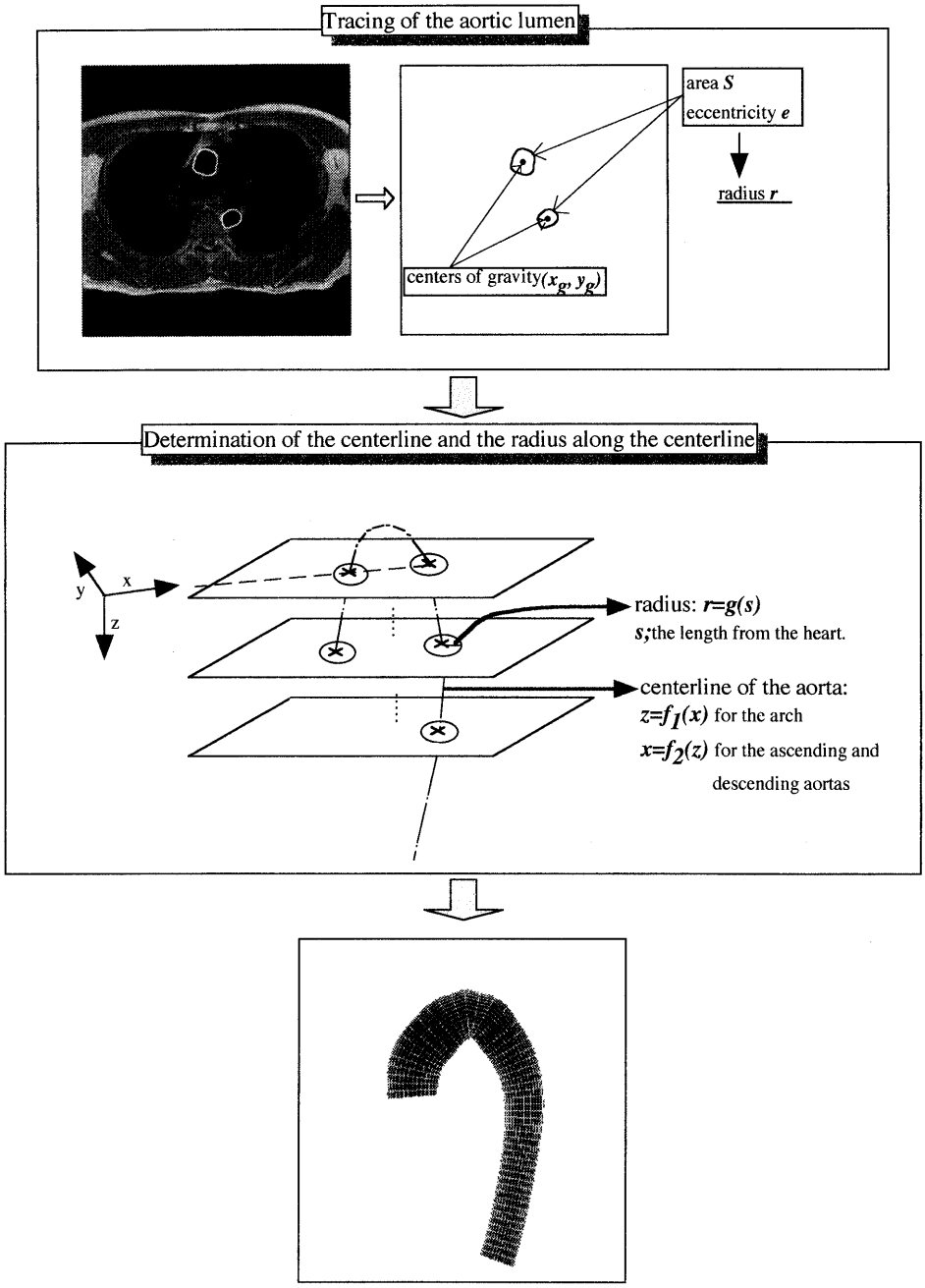

Fig. 2 The outline of the model construction

for the descending aorta ; where x and z are the x and z coordinates in mm, respectively.

2.2.3 Radius change along the centerline Generally speaking, the luminal shape of the aorta in MRI images is elliptic. If the shape of the section of the aortic lumen perpendicular to the centerline of the aorta is a circle with radius r, the shape of any sections which have an arbitrary angle to the centerline is an ellipse whose length of the shorter semi-axis b is equal to r. We thus used the length of the shorter semi-axis b as the radius r, and calculated it from the area S and the eccentricity e of each lumen. The eccentricity e was defined as Eq.(1), where the length of the longer and shorter semi-axes corresponded to l_l and l_s in Eq.(1), respectively. The area of the ellipse S is defined as

$$S=\pi ab \tag{5}$$

where a is the length of the longer semi-axis. From Eqs.(1) and (5), we got

$$b=r=\sqrt{\frac{S\sqrt{1-e^2}}{\pi}}. \tag{6}$$

The radius r(mm) was approximated with a 4-degree polynomial function of the distance from the heart s (mm) :

$$r=-1.47\times10^{-8}s^4+8.39\times10^{-3}s^3$$

$$-1.50\times10^{-3}s^2+6.28\times10^{-2}s+13.3 \quad (7)$$

where r is the radius of the aorta, and s is the distance from the heart. The distance s was calculated by summing up the length between the points along the centerline from the position closest to the heart. The correlation coefficient between the data and the equation was about 0.98. The radius r was about 13 - 15 mm at the ascending aorta, and was about 9 - 11 mm at the descending aorta.

2. 2. 4 Wall thickness It was difficult to evaluate the wall thickness because 1 pixel was corresponding to about 1 mm in the image. The wall thickness in the model was set at 2 mm at any position.

2. 2. 5 Consideration of the branches It was difficult to identify the luminal shape of the branches from the thoracic aorta in the MRI images. We approximated the branches, i.e., the brachiocephalic trunk, the left common carotid artery, the left subclavian artery, and the intercostal arteries as beams. The length and the radius of these beams at the aortic arch were 70 mm and 2 mm, respectively. The branching end of the left carotid artery was at the top of the aortic arch and this beam was parallel to the body axis (z axis). The distance between the branching ends of the brachiocephalic trunk and the left common carotid artery was about 10 mm, and the angle between them was 45 degree. The left subclavian artery and the branchiocephalic trunk were symmetric about the left common carotid artery. The intercostal arteries were modelled as 12 pairs of beams whose length and radius were 10 mm and 1 mm, respectively. The distance between each pair was 4 mm and each pair made 60 degree.

2. 3 Construction of models with aneurysms

The models with aneurysms were made to study the effects of the aortic aneurysm on the stress distribution of the aorta preliminarily. In this study, we examined the effect of the position and the eccentricity of the aneurysm. A fusiform bulge was made in each model by increasing the radius of the normal model locally. The wall thickness of the model was the same as that of the normal model. The maximum radius was 5 cm, the critical diameter for the aneurysm operation. The shape of the section was obtained at intervals of about 4 mm along the centerline as explained in Section 2 - 4. We defined the region of the aneurysm using 11 sections, hence the axial length of the aneurysm was 4 - 5 cm in each model. The axial length was not constant, because the aortic axis was not straight. The aneurysm was divided into the upper and the lower regions. Trigonometric functions were utilized to connect the aneurysm region to the normal aortic region smoothly.

In the upper and lower regions of the aneurysm, we used the following functions, respectively:

$$r=r_u+(25-r_u)\times\sin\left(\frac{\pi}{10}n\right) \quad (0\leq n\leq5) \quad (8)$$

$$r=r_l+(25-r_l)\times\sin\left(\frac{\pi}{10}(10-n)\right) \quad (5\leq n\leq10) \quad (9)$$

where r_u (mm) and r_l (mm) are the radii of the normal aorta at the uppermost and lowermost section respectively, r (mm) is the radius of the aneurysm at the each section, and n is the serial number of the sections being the uppermost section 0.

Each model had one aneurysm in the ascending aorta, the descending aorta, or the aortic arch adjacent to the descending aorta. The model with the aneurysm in the ascending aorta was named model As. Similarly, the model with the aneurysm in the descending aorta was named model Ds and the model with the aneurysm in the aortic arch adjacent to the descending aorta was named model AD. In models Ds and AD, the centerline of the aneurysm was tortured to make the back side of the aneurysm in plane with the aorta, considering the constraint by the vertebral column. In model As, the aneurysm was concentric with the aorta. To investigate the effect of the eccentricity, we also made a model with an asymmetric aneurysm of the ascending aorta and called model Ase.

2. 4 Finite element analysis

The models obtained in Sections 2.2 and 2.3 were discretized and meshed for the finite element analysis: First, we selected the sections perpendicular to the centerline at intervals of 4 mm in the ascending and the descending aortas. In the aortic arch, we selected 5 sections perpendicular to the centerline by dividing the aortic arch into 6 parts with equal length along the centerline. The distance between each section was about 4 mm. The sections form the inner surface. The outer surface was defined with the sections whose radius was 2 mm longer than that of the inner surface. The coordinates of the total of 72 points at the inner and outer surfaces were obtained for each section at intervals of 10 degree. From these points, the wall of the aorta was defined as a set of hexahedrons. The number of the elements was about 2000 and that of the nodes was about 14000. We used ANSYS ver. 5.5 (Swanson Analysis Systems, Inc.) for the analysis on a work station (Sun Ultra 10, Sun Microsystems, Inc.).

We used the solid element with 20 nodes for the aortic wall and the beam elements for branches. They were isotropic and had linear elasticity. Examples of the meshing of the normal model and model As are shown in Fig. 3 and Fig. 4 respectively. In addition, their Poisson's ratio was set at 0.4999 to mimic the

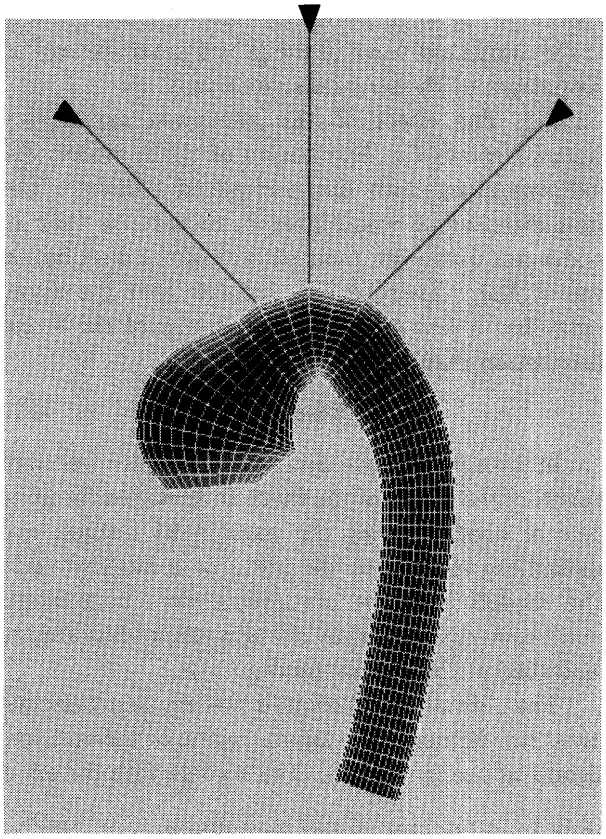

Fig. 3 The example of meshing in an aneurysm model (Model As). Solid triangles indicate that the translational but not rotational movement is constrained completely. The intercostal arteries were constrained similarly.

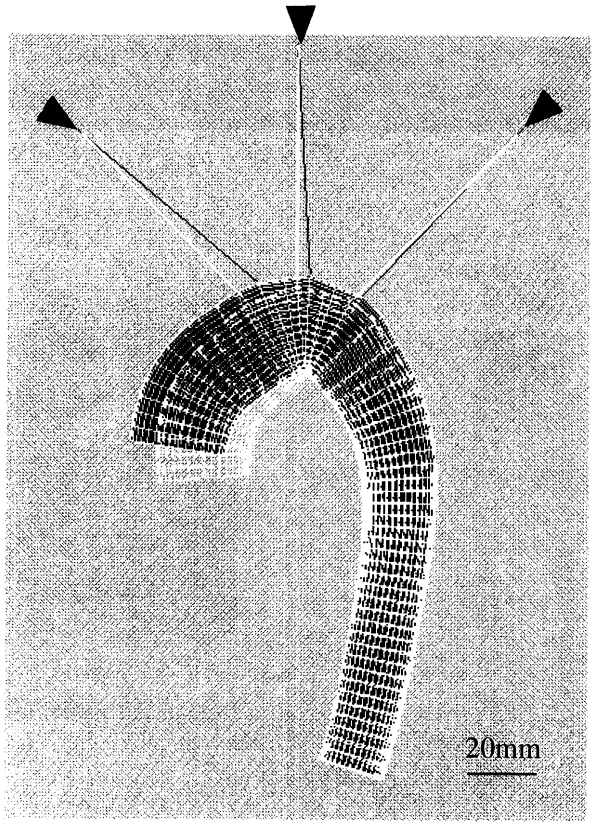

Fig. 4 The normal model before (white line) and after (dark surface) applying the pulse pressure. Solid triangles indicate that the translational but not rotational movement is constrained completely. The intercostal arteries were constrained similarly.

incompressibility of the wall material. Young's modulus of the aorta and aneurysm was set at 4.68 MPa, referring the tensile test data of the normal and aneurysmal tissues of the aorta by in Raghavan et al.[5] They divided stress-strain curves into two phases and calculated the Young's modulus in each phase. We used the modulus of the normal tissue in the higher strain phase, for the modulus was not significantly different between the normal and aneurysmal tissues. Young's modulus of the beam in the normal model and the beam in the model with the aneurysm were set at 20.0 MPa. One end of each beam was on the outer surface of the aorta and had the same movement as the surface. The other end was constrained completely in the translational movenent but not in the rotational movement. The regions near the heart and the diaphragm were not constrained. The blood pressure of the subject was 117 mmHg in the systole and 75 mmHg in diastole. Hence the difference of the pressure was 42 mmHg. We set the pressure applied to the inner surface of the aorta at 42 mmHg.

3. Results

We developed the simple method to construct finite element models of aortas from the axial MRI images. In this method, we could construct the model of the aorta, based on the parameters such as the center of the gravity, the eccentricity, and the area of the aorta observed in each image.

3.1 The normal model

Figure 4 shows the shape change of the normal model due to pressurization. The ascending aorta seemed to deform more than the descending aorta. The aortas of other models deformed similarly. Distribution of the first principal stress S1 in the normal model is shown in Fig. 5. The inner side wall of the aortic arch had the maximum value of the 1st principal stress.

3.2 Models with aneurysms

3.2.1 The effect of the aneurysm position

Figure 6 shows the distribution of S1 in models Ase, AD, and Ds along with the maximum of the first principal stress, S1max normalized by that in the normal model. We selected model Ase, not As, because Ase had the same degree of the eccentricity

as models AD and Ds. The normalized S1max was varied with the models and is highest in model AD. However the pattern of the stress distribution in the models was similar. These results indicate that the position of the aneurysms may have a stronger effect on the maximum value of the principal stress than on the pattern of the stress distribution.

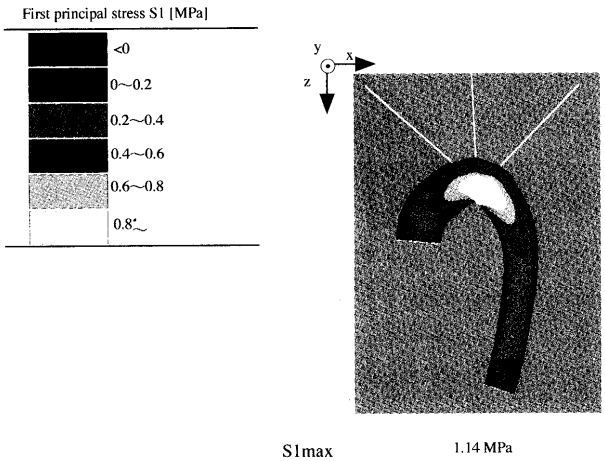

Fig. 5 The stress distribution in the normal model. S1, first principal stress; S1max, the maximum value of the first principal stress

3.2.2 The effect of the aneurysm asymmetry Figure 7 shows the distribution of S1 in models As, and Ase along with the normalized S1max. The normalized value was higher in model Ase than in model As. However, their pattern of the distribution was similar. These results indicate that the asymmetry has a less effect on the pattern of the stress distribution than on the value itself.

4. Discussion

In this research, we developed a simple method to construct the model of the thoracic aorta for the finite element analysis using the axial MRI images, and applied the method to the aorta of a healthy male. The models with the aneurysms were constructed from the normal model by changing the radius and the centerline of the normal model.

The normal model showed that the first principal stress was higher in the lateral region of the arch and highest at the inner wall. The models with the aneu-

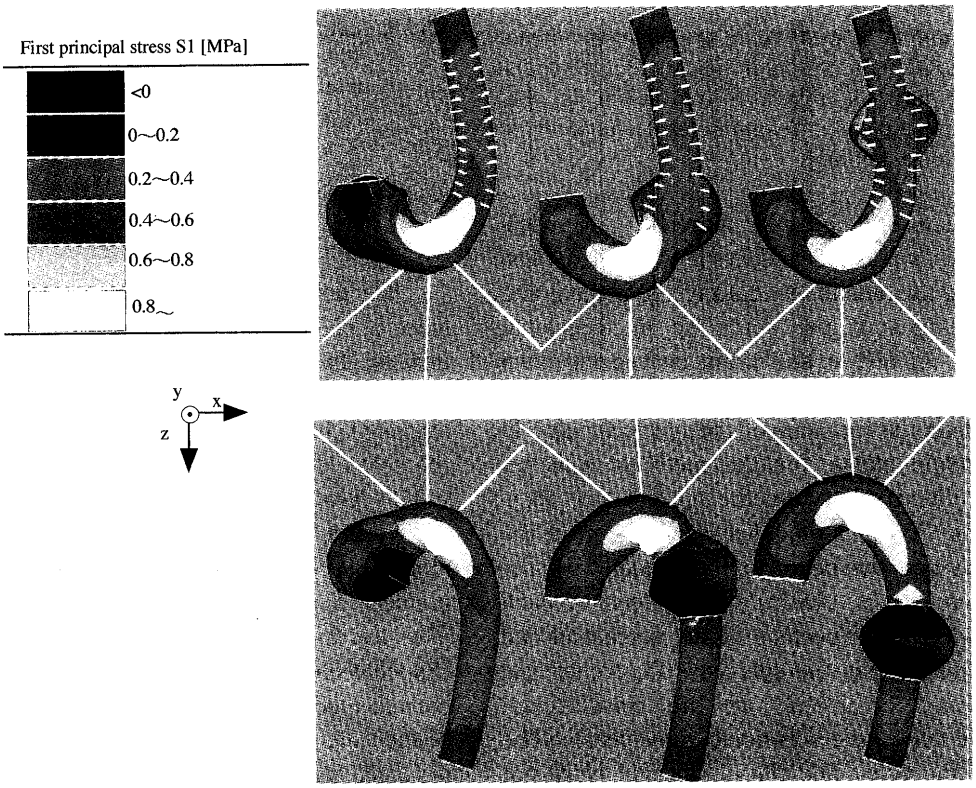

Fig. 6 The stress distribution in the aneurysm models. S 1, first principal stress; normalized S 1max, the maximum value of the first principal stress normalized by the maximum value in the normal model

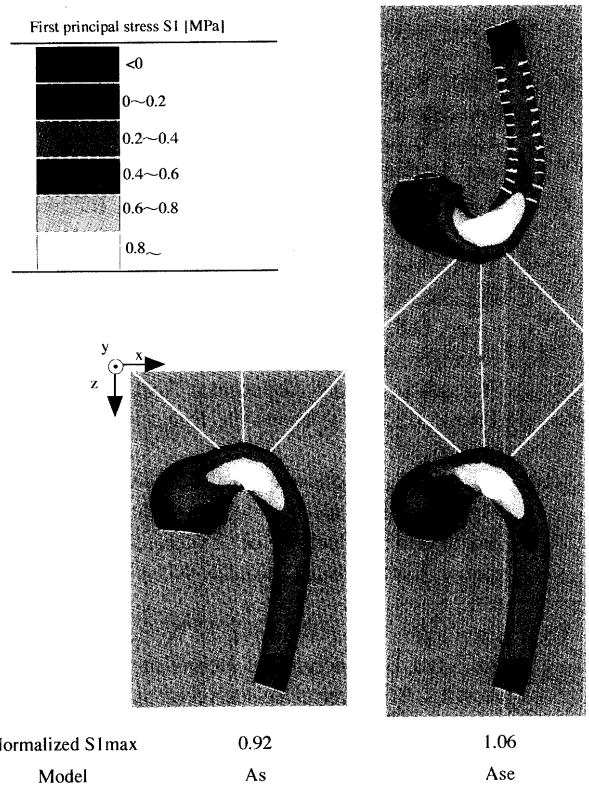

Fig. 7 The stress distribution in the aneurysm models. S1, first principal stress; normalized S1max, the maximum value of the first principal stress normalized by the maximum value in the normal model

rysms showed the same tendency. These results indicate that the lateral to the inner wall of the aortic arch may have the highest potential to rupture if the strength of the aorta does not vary with the position. The aortic aneurysms preferentially initiate at the aortic arch near the descending, like the aneurysm in the model AD, which is closest to the position of the highest stress and the high stress region of all models. The high stress spread from the inner to the lateral side might involve the development of the aneurysm.

The first principal stress was highest in the model AD, suggesting that the aneurysm at the region between the arch and the descending aorta has higher potential to rupture than the aneurysms at the ascending and the descending aortas have. The maximum value of the model Ase was higher than that of the model As. The result showed that the eccentricity in the aneurysm increased the maximum value of the first principal stress. Such an effect of eccentricity agrees with clinical observation[6]. The maximum value of the first principal stress varied with the model, whereas the pattern of the stress distribution did not. The result showed that the eccentricity, the position of the aneurysm had a stronger effect on the maximum value of the first principal stress than on the pattern of the stress distribution.

We used the first principal stress in each model to evaluate the potential of rupture. There would be other parameters including von Mises stress and maximum shear stress for this purpose. In these parameters, the most appropriate parameter has not been known yet. Although a hydrostatic pressure is not usually used for the material failure, it may be useful for that purpose, because vasa vasorum are collapsed by the high hydrostatic pressure, which may lead to tissue necrosis and softening of the wall material. We are now planning to study the failure properties of the aneurysmal tissue to find out the suitable parameters.

The most of the time of the analysis was occupied by tracing the aortic lumens. This process could not be improved for the moment, because the MRI images were not clear enough to detect the inner surface automatically. Also the resolution of the images was not high enough to identify the intraluminal shape of the branch. It is necessary to model the branches, especially those at the aortic arch, with the same elements and manner as the aortic wall for future analysis, because the aneurysm often involves these branches. The wall thickness was assumed to be uniform through the entire wall, because 1) we concentrated on the effect of the position and the eccentricity of the aneurysm as the first step, not the variation of the wall thickness, and 2) it was impossible to obtain the wall thickness from the MRI images. Of course it is very important to consider the wall thickness variation. We need to take it into consideration in the future analysis, once reliable data of the wall thickness become available. The assumption that the shape of the inner surface of the aorta perpendicular to the centerline of the aorta is a circle might not be valid for the complex shape of the actual aneurysms. The problem could be solved by using a function which could be applied to various shapes such as B spline. Also the centerline has to be defined three dimensionally if the shape of the aorta is complex. In this investigation, we estimated the stress distribution of the aorta when the inner surface was pressurized. This analysis is the first step to estimate the stress distribution in aortic aneurysms. The effect of blood flow on the stress distribution in aneurysmal walls should be included in the future analysis. We approximated the branches as the beam elements, and the edges opposite to the surface of the aorta were constrained translationally. But we do not know whether this constraint is proper or not, because the tethering force and the movement of the heart are not known yet. The proper constraint is under investigation. We assumed that the elements were isotropic

and linearly elastic, and had no residual stress. However, it is well known that blood vessel walls show marked nonlinearity and anisotropy in their mechanical stress. Further, the importance of residual stress has been pointed out for stress analysis in arterial walls. Since there is some possibility that the stress distribution of the wall is changed by considering these mechanical parameters, we need to include them for the stress analysis in the future.

In this study, we developed a simple method to construct models of the whole thoracic aorta and analyzed the stress distribution in the model of the normal thoracic aorta and the models with fusiform bulges. We need to construct models based on the actual shape of aneurysms for future analysis, which would enable us to evaluate the rupture potential of the aneurysm in each patient. Additionally, this method may become an important tool for the planning of treatment strategies for aneurysms, especially when a patient has multiple aneurysms and there is a need to establish priorities among them.

Acknowledgments

This work was supported in part by Grants-in-Aid from the Ministry of Education, Science and Culture in Japan (Nos. 10480241 and 1180834) and the Circle for the Promotion of Science and Engineering.

References

(1) Inzoli, F., Boschetti, F., Zappa, M., Longo, T. and Fumero, R., Biomechanical Factors in Abdominal Aortic Aneurysm Rupture, Eur. J. Vasc. Surg. Vol. 7 (1993), pp. 667-674.

(2) Kyriacou, S.K. and Humphery, J.D., Influence of Size, Shape and Properties on the Mechanics of Axisymmetric Saccular Aneurysms, J. Biomech., Vol. 29, No. 8 (1996), pp. 1015-1022.

(3) Elger, D.F., Blackketter, D.M., Budwif, R.S. and Johansen, K.H., The Influence of Shape on the Stresses in Model Abdominal Aortic Aneurysms, Trans. ASME, J. Biomech. Eng., Vol. 118 (1996), pp. 326-332.

(4) Vorp, D.A., Raghavan, M.L. and Webster, M.W., Mechanical Wall Stress in Abdominal Aortic Aneurysm: Influence of Diameter and Asymmetry, J. Vasc. Surg., Vol. 27, No. 4 (1998), pp. 632-639.

(5) Raghavan, M.L., Webster, M.W. and Vorp, D.A., Ex Vivo Biomechanical Behavior of Abdominal Aortic Aneurysm: Assessment Using a New Mathematical Model, Ann. Biomed. Eng., Vol. 24 (1996), pp. 573-582.

(6) Taylor, B.V. and Kalman, P.G., Saccular Aortic Aneurysm, Ann. Vasc. Surg., Vol. 13 (1999), pp. 555-559.